ISSN 1070-3284, Russian Journal of Coordination Chemistry, 2015, Vol. 41, No. 5, pp. 305–311. © Pleiades Publishing, Ltd., 2015.

Three-Dimensional 3*d*–4*f* Frameworks Constructed through Substituted Imidazole-Dicarboxylate: Synthesis, Structure, and Characterization[1]

X. Feng[a, *], C. L. Wang[b], J. Zhao[b], S. Y. Xie[a], L. Y. Wang[a, b] and Seik-Weng Ng[c]

[a] *College of Chemistry and Chemical Engineering, Luoyang Normal University, Luoyang, 471022 P.R. China*

[b] *School of Life Science and Technology, Nanyang Normal University, Nanyang, 473601 P.R. China*

[c] *Department of chemistry, University of Malaya, Kuala Lumpur, 50603, Malaysia*

**e-mail: fengx@lynu.edu.cn*

Received September 27, 2014

Abstract—A heteronuclear metal organic framework containing erbium(III) and cobalt(II) ion based on a rigid ligand of substituted imidazoledicarboxylic acid has been synthesized and characterized by single-crystal X-ray diffraction analysis (CIF file CCDC no. 1019455). It's formula is $[Er_2Co_2(\mu_3\text{-HMimda})_2(\mu_3\text{-Mimda})_2 \cdot 4H_2O]_n \cdot 2nH_2O$, ($H_3$Mimda = 1-*H*-2-methyl-4,5-imidazole-dicarboxylic acid). The complex crystallizes in the monoclinic system. It possesses an extended grid-like porous structure constructed from corrugated shaped 2D layer. Direct current magnetic susceptibility measurements for indicated the depopulation of the Stark components at low temperature and possible very weak antiferromagnetic interactions within heteronuclear MOF.

DOI: 10.1134/S1070328415040016

INTRODUCTION

In recent years, the rational design and construction of 3*d*–4*f* heterometallic coordination polymers have provoked the interest of chemists not only due to their potential applications in the fields of magnetism, luminescence, gas adsorption, and bimetallic catalysis, but also their fascinating architectures and arrays [1–3]. From the magnetic viewpoint, molecular magnetic materials based on transition metal ions, such as Co^{2+} have been extensively studied because the high spin ground state can be obtained from strong exchange interaction between 3*d* electrons. However, a high spin ground state and significant magneto anisotropy cannot be simultaneously achieved easily in 3*d* complexes due to the small spin-flip. The magnetic properties of large magnetic anisotropy of lanthanides continue to be an attractive research field because of their unique and intriguing properties and potential applications in molecular spintronics [4]. Couplings between the lanthanide and transition metallic ions (*f*–*d*) are much stronger than *f*–*f* interactions, and the combination of such two kinds of spin carriers into a singular material may help to improve their magnetic properties in heterometallic materials [5]. However, no systematic investigation of zeolite-type functional materials containing lanthanide metal atoms series along with the transition metal atoms has been documented systematically [6], and Ln–Co heteronuclear metal organic frameworks (MOFs) with 3D framework structures have been seldom reported yet. This is due to the practically challenging syntheses of 3*d*–4*f* heterometallic MOFs. One of the difficulties is how to control the variable coordination environment of the lanthanide ions [7]. As continuation of our previous research [8], we have extended this idea by application of a simple H_3Mimda ligand for construction of heterometallic MOFs $[Er_2Co_2(\mu_3\text{-HMimda})_2(\mu_3\text{-Mimda})_2 \cdot 4H_2O]_n \cdot 2nH_2O$ (**I**) (H_3Mimda = 1-*H*-2-methyl-4,5-imidazole-dicarboxylic acid) with novel architectures and interesting properties.

EXPERIMENTAL

Materials and physical measurements. Lanthanide oxides were purchased from Jinan Henghua Sci. & Tec. Co. Ltd. Erbium nitrate was prepared by the reaction of erbium oxides and nitric acid (11 mol/L). Elemental analyses (C, H, and N) were performed on a PerkinElmer 2400 element analyzer. IR spectra were recorded in the range 400–4000 cm^{-1} using a VECTOR-22 spectrometer using KBr discs. Magnetic data were obtained using a Quantum Design MPMS SQUID 7S magnetometer at an applied field of 2000 Gs using multicrystalline samples in the temperature range of 1.8–300 K. The magnetic susceptibilities were corrected using Pascal's constant for all the constituent atoms and sample holders. Thermogravimetric (TG) and differential thermal analysis (DTA) experiments were performed using a TGA/NETZSCH STA449C instrument heated from 25–900°C (heating rate of 10°C/min in nitrogen stream). The powder

[1] The article is published in the original.

Table 1. Crystallographic data and experimental details for compound **I**

Parameter	Value
Formula weight	633.99
Temperature, K	293(2)
Crystal system	Triclinic
Space group	$C2/c$
a, Å	24.0431(12)
b, Å	9.0516(5)
c, Å	18.7594(9)
β, deg	114.5062(6)
Volume, Å^3; Z	3714.8(3); 8
ρ_{calcd}, g/cm^3	2.267
Absorption coefficient, mm^{-1}	5.449
Index ranges	$-31 \le h \le 28$, $0 \le k \le 11$, $0 \le l \le 24$
F(000)	2448
θ Range for data collection, deg	1.86–27.50
Independent reflections	4098
Observed reflections	10124
Data/restraints/parameters	4098/0/255
Goodness-of-fit on F^2	1.264
R index ($I > 2\sigma(I)$)*	$R_1 = 0.0367$, $wR_2 = 0.1221$
R index (all data)*	$R_1 = 0.0441$, $wR_2 = 0.1529$
Largest diff. peak/hole, e Å^{-3}	2.487/−3.096

* $R = [\Sigma\|F_o| - |F_c\|/\Sigma|F_o|]$, $R_W = \Sigma_W[|F_o^2 - F_c^2|^2/\Sigma_W(|F_w|^2)^2]^{1/2}$.

X-ray diffraction (PXRD) patterns were measured have been performed at room temperature using a Bruker D8 advance powder diffractometer at 40 kV, 40 mA for CuK_α radiation (λ = 1.5418 Å).

Synthesis of I. Cobalt nitrate hexahydrate (0.029 g, 0.1 mmol) and erbium(III) nitrate hexahydrate, (0.046 g, 0.1 mmol) were mixed in a water solution (10 mL) of H_3Mimda (0.3 mmol, 0.079 g). After stirring for 30 min in air, the aqueous mixture was placed into 25 mL Teflon-lined autoclave under autogenous pressure being heated at 155°C for 72 h, and then the autoclave was cooled over a period of 24 h at a rate 5°C/h, and pink crystals were obtained suitable for X-ray diffraction analysis. The yield was 0.0416 g (53%) based on erbium element.

For $C_{13.5}H_{14.5}CoErN_{4.5}O_{10.5}$

anal. calcd., C, 25.58; H, 2.31; N, 9.94; Co, 9.30; Er, 26.38. %:

Found, %: C, 24.59; H, 2.16; N, 9.63.

IR (KBr; ν, cm^{-1}): 3471 br, 3140 s, 2453 m, 1612 v.s, 1473 s, 1396 s, 1265 s, 1126 s, 883 s, 787 s.

X-ray crystallography. Single crystal diffraction data of title complex were collected on a Bruker SMART APEX II CCD diffractometer with graphite-monochromated MoK_α radiation (λ = 0.71073 Å) at room temperature. The structures were solved using direct methods and successive Fourier difference synthesis (SHELXS-97), and refined using the full-matrix least-squares method on F^2 with anisotropic thermal parameters for all nonhydrogen atoms (SHELXL-97) [9]. An empirical absorption correction was applied using the SADABS program. These reflections are in the ranges of $-31 \le h \le 28$, $0 \le k \le 11$ and $0 \le l \le 24$ with $2\theta_{max} = 55.0°$. The hydrogen atoms of organic ligands were placed in calculated positions and refined using a riding on attached atoms with isotropic thermal parameters 1.2 times those of their carrier atoms. The maximum and minimum main axis ADP ratio (Angstrom Units) is tested for the main residue, large value may indicate unresolved disorder of solvate, which is difficult identify. Solvate molecules were accounted for by using the program PLATON/SQUEEZE (Spek, 2009), as the result, there are parameters discrepancies between the given and expected value. All non-hydrogen atoms were refined with anisotropic thermal parameters. The final $R = 0.0441$, $wR = 0.1529$ ($w = 1/[\sigma^2(F_o^2) + (0.0852P^2) + 26.6113P]$, where $P = (F_o^2 + 2F_c^2)/3$), $(\Delta\rho)_{max} = 0.536$ and $(\Delta\rho)_{mix} = -0.467$ e/Å^3. Crystallographic and experimental details are summarized in Table 1, and the selected bond lengths and bond angles are listed in Table 2.

Supplementary material for structure **I** has been deposited with the Cambridge Crystallographic Data Centre (no. 1019455; deposit@ccdc.cam.ac.uk or http://www.ccdc. cam.ac.uk).

RESULTS AND DISCUSSION

Stoichiometries of **I** have been confirmed by single X-ray crystallography, elements analysis and thermogravimetric analysis. Fig. 1 gives a perspective view of the basic unit in complex **I** together with atomic labeling system. The asymmetry unit contains one Er^{3+} ion, one Co^{2+} ion, four HMimda ligands and two coordinated waters, as well as two free water molecules. The octa-coordinated Er^{3+} cation exhibits distorted dodecahedral prism geometry, being accomplished by an O_8 donor set, among which two oxygen atoms are from water molecules, and another six are from imidazole carboxylic groups. HMimda ligands connected adjacent three metal ions in both bridging and chelating fashions (a, b). Diverse coordination modes of H_3Mimda ligand in complex **I** are the following:

Table 2. Selected bond lengths (Å) and angles (deg) for complex **I**

Bond	*d*, Å	Bond	*d*, Å	Bond	*d*, Å
Er(1)–O(7)$^{\#1}$	2.189(5)	Er(1)–O(6)$^{\#1}$	2.364(6)	Co(1)–O(8)$^{\#3}$	2.096(5)
Er(1)–O(3)	2.228(5)	Er(1)–O(6)	2.497(5)	Co(1)–N(4)$^{\#3}$	2.107(7)
Er(1)–O(1)	2.259(5)	Co(1)–N(2)$^{\#2}$	2.046(6)	Co(1)–O(4)$^{\#2}$	2.143(5)
Er(1)–O(2*w*)	2.300(6)	Co(1)–N(1)	2.055(6)	Co(1)–O(2)	2.159(5)
Er(1)–O(1*w*)	2.335(6)				
Er(1)–O(6)	2.497(5)				
Angle	ω, deg	Angle	ω, deg	Angle	ω, deg
O(7)$^{\#1}$Er(1)O(3)	78.4(2)	O(8)$^{\#3}$Co(1)N(4)$^{\#3}$	77.2(2)	O(7)$^{\#1}$Er(1)O(5)	165.1(2)
O(7)$^{\#1}$Er(1)O(2*w*)	82.5(3)	N(2)$^{\#2}$Co(1)O(4)$^{\#2}$	78.2(2)	O(3)Er(1)O(5)	94.2(2)
O(3)Er(1)O(2*w*)	135.7(2)	O(7)$^{\#1}$Er(1)O(1)	106.2(2)	O(1)Er(1)O(5)	84.4(2)
O(1)Er(1)O(2*w*)	146.3(2)	O(2*w*)Er(1)O(1*w*)	71.0(2)	O(2*w*)Er(1)O(5)	94.4(2)
O(7)$^{\#1}$Er(1)O(1*w*)	89.0(2)	O(7)$^{\#1}$Er(1)O(6)$^{\#1}$	76.69(19)	O(1*w*)Er(1)O(5)	76.2(2)
O(3)Er(1)O(1*w*)	69.1(2)	O(3)Er(1)O(6)$^{\#1}$	135.53(18)	O(6)$^{\#1}$Er(1)O(5)	116.83(17)
O(1)Er(1)O(1*w*)	139.9(2)	O(1)Er(1)O(6)$^{\#1}$	74.72(19)	N(2)$^{\#2}$Co(1)N(1)	93.8(3)
O(7)$^{\#1}$Er(1)O(6)	139.57(19)	O(2*w*)Er(1)O(6)$^{\#1}$	76.0(2)	N(2)$^{\#2}$Co(1)O(8)$^{\#3}$	91.7(2)
O(3)Er(1)O(6)	139.31(19)	O(1*w*)Er(1)O(6)$^{\#1}$	145.41(19)	N(1)Co(1)O(8)$^{\#3}$	164.3(2)
O(1)Er(1)O(6)	76.95(17)	O(5)Er(1)O(6)	52.1(2)	N(1)Co(1)O(2)	77.9(2)
O(2*w*)Er(1)O(6)	76.00(19)	N(4)$^{\#3}$Co(1)O(4)$^{\#2}$	95.6(2)	O(8)$^{\#3}$Co(1)O(2)	86.8(2)
O(1*w*)Er(1)O(6)	114.9(2)	N(2)$^{\#2}$Co(1)O(2)	98.6(2)	N(4)$^{\#3}$Co(1)O(2)	88.3(2)
O(6)$^{\#1}$Er(1)O(6)	65.15(18)	N(1)Co(1)O(4)$^{\#2}$	98.5(2)	O(4)$^{\#2}$Co(1)O(2)	175.1(2)
N(2)$^{\#2}$Co(1)N(4)$^{\#3}$	166.6(3)	O(3)Er(1)O(1)	77.8(2)	O(8)$^{\#3}$Co(1)O(4)$^{\#2}$	97.0(2)
N(1)Co(1)N(4)$^{\#3}$	98.8(3)				

* Symmetry codes: $^{\#1}$ $-x+1, -y+1, -z+1$; $^{\#2}$ $-x+1/2, y-1/2, -z+1/2$; $^{\#3}$ $-x+1, y, -z+1/2$; $^{\#4}$ $-x+1/2, y+1/2, -z+1/2$.

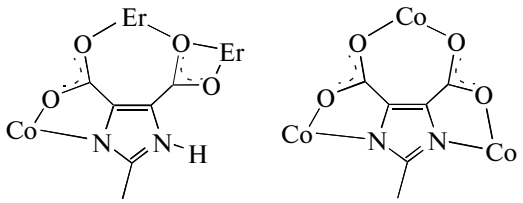

(a) (b)

As far as the Co^{2+} ion is concerned, it exhibits an octahedron geometry, being coordinated by three HMimda ligands. Each HMimda ligand provides on oxygen and one nitrogen atom, and Co^{2+} ions is located in S_3 symmetry position. It just demonstrates slightly different coordination environment, being compared with the simple Co(II) complex for the bond lengths and angles [11]. The multidentate functionality of $HMimda^-$ and the tendency of Er(III) to have a high coordination number allowed water molecule to act as a terminal ligand to Er^{3+} ions in title complex [12].

Two adjacent Er^{3+} ions are doubly bridged by two 5-carboxylic group of from $HMimda^-$ ligand to form a dimer unit in an *anti-anti* chelating mode with the separation of Er···Er of 4.097 Å. At the same time, the 4,5-carboxylic groups connect adjacent Co^{2+} ions into binuclear unit with the shortest distance Co···Co of 6.304 Å. Four $Mimda^{2-}$ ligand alternately linked two adjacent Er^{3+} ions and Co^{2+} ions into a heterometallic $[ErCo(Mimda)_4]$ aggregate as the secondary building unit (SBU) through the carboxylic oxygen and imidazolyl nitrogen. Meanwhile, two $Mimda^{2-}$ ligands connected neighboring four Er^{3+} ions, gives a square lanthanide cluster. The carboxylate further propagate the clusters above mentioned into one dimensional (1D) robust polymeric chain approximately along crystallographic *yz* plane, as described in Fig. 2.

The carboxylic oxygen atoms crosslink these 1D chains into 2D corrugated-shape layer approximately along crystallographic *xz* plane, as illustrated in Fig. 3a. Moreover, the carboxylic oxygen and imidazolyl nitrogen atoms from two $Mimda^{2-}$ ligands further interconnected 2D layer sheet, giving rise the finally 3D reticular three-dimensional (3D) coordination frameworks, as described in Fig. 3b. These coplanar rigid ligands always render short separation between adja-

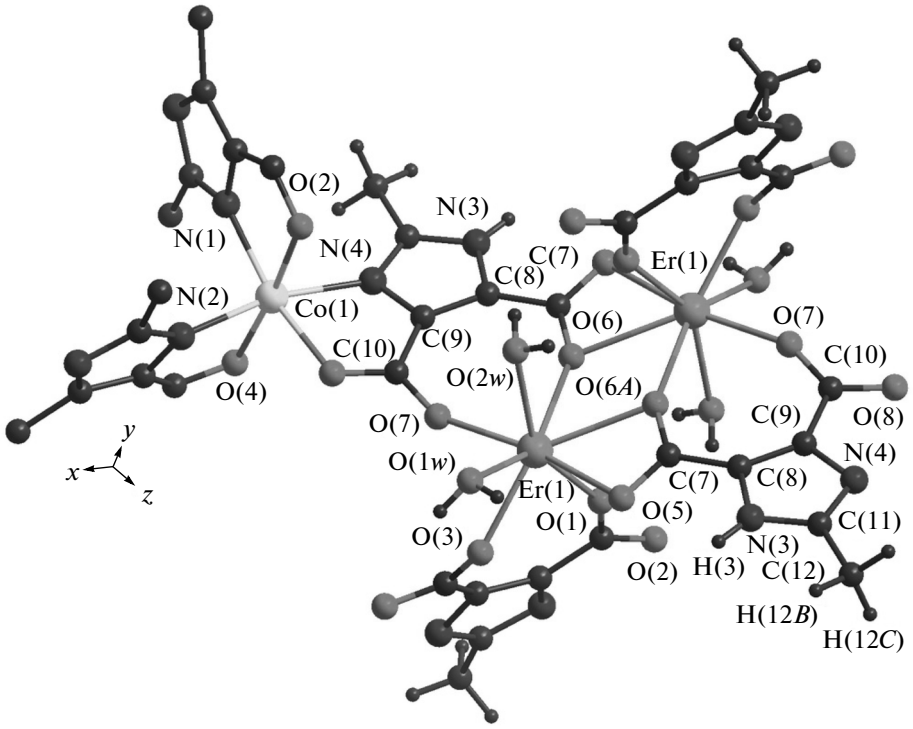

Fig. 1. Coordination environments of the Er^{3+} and Co^{2+} cations with partial atomic labels in complex **I**.

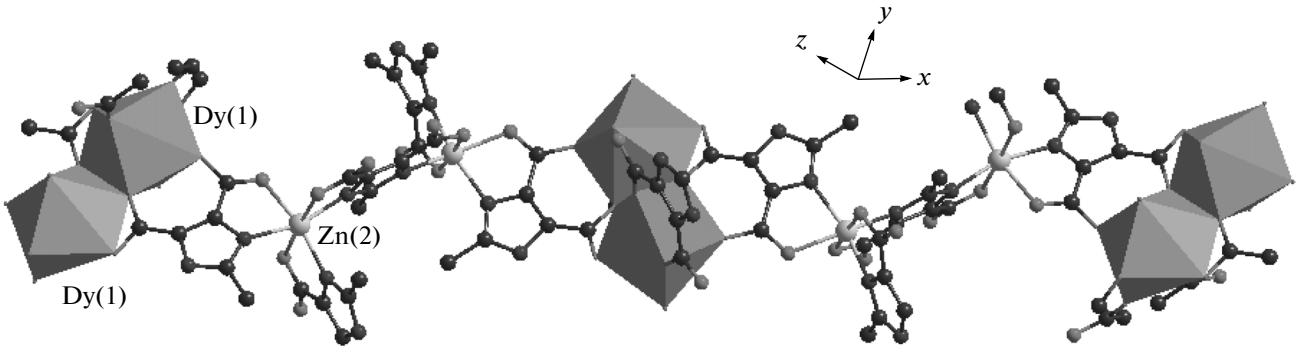

Fig. 2. View of 1D alternate metallic cluster chain structure in **I**.

cent metal ions, facilitating energy transition to the Er(III) centers, resulting in their potential applications in the areas of magnetic and electroluminescent devices [13]. The framework possesses 1D channel along the *z* axis with a window diameter of about 7.55 Å, which is occupied by the both coordinated and solvate water molecules. This porous assemble is much different from the reported pure lanthanide or transition metal complex based on analogous ligand [14]. After hypothetical removal of the guest and coordinated waters, the total potential solvent accessible void is found for the 3D noninterpentrating framework to be 296.2 $Å^3$ percell volumes (accounting for 16.7% of the total unit cell system), calculated using the PLATON/SQUEEZE programmes [15].

The powder XRD pattern of complex **I** feature first hump at $2\theta = 5.68°$ and distinct peaks at $2\theta = 11.2°$, 14.6°, 17.3°, 22.4°, 25.4° and 37.3°. The experimental PXRD patterns of bulk complex nearly match with the calculated patterns obtained from corresponding single crystal structures.

To characterize the thermal stability of complex **I**, TG analysis and DTA differential thermal analysis have been carried out, as reported in Fig. 4. It shows an endothermic peak in the range of 110–130°C with a weight loss of 4.44%. This was caused by the release of two lattice water molecules performula, and the re-

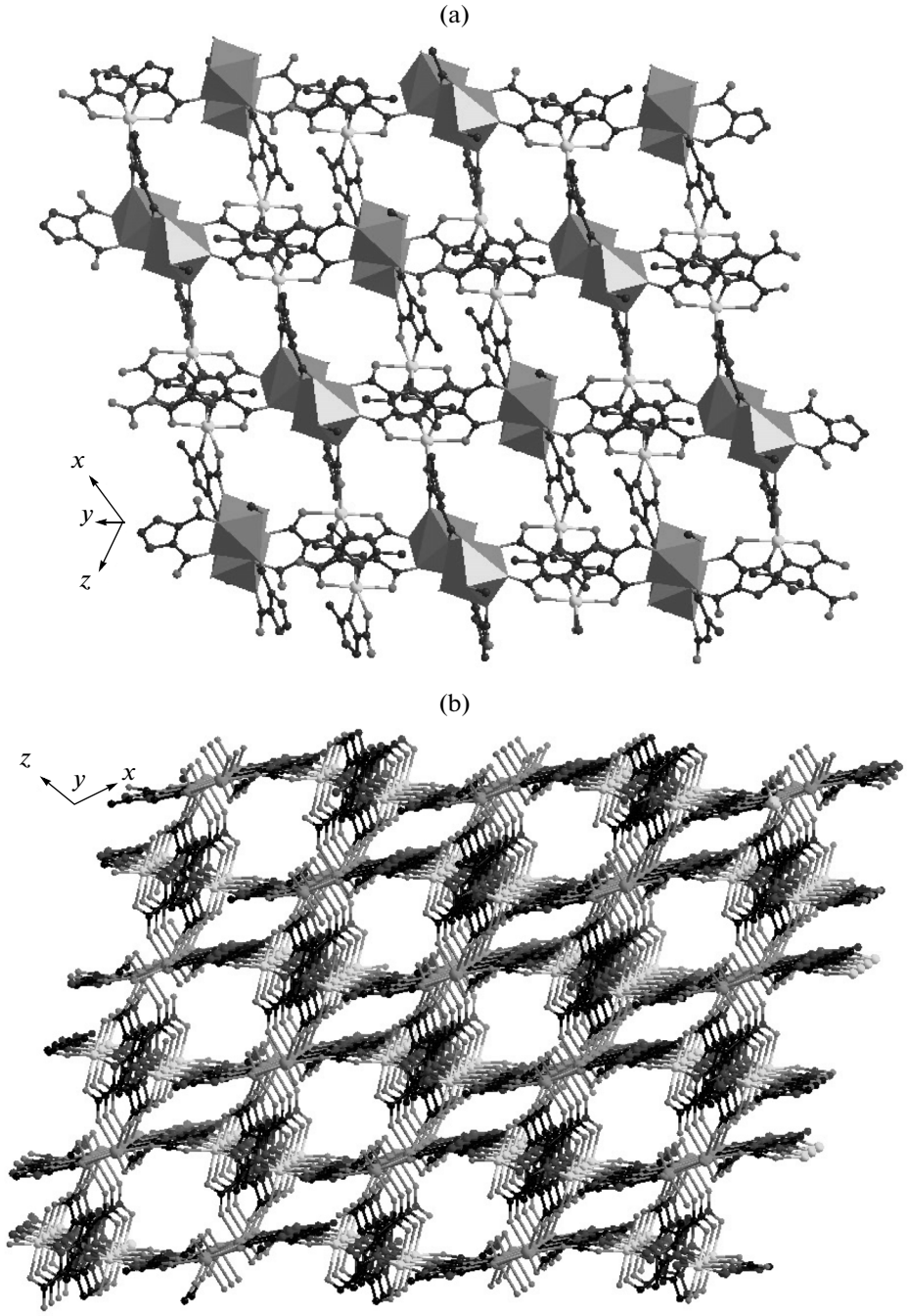

Fig. 3. Polyhedral view of corrugated-shaped 2D layer constructed from Er_2Co_2 SBUs (a); crystal packing diagram of 3D reticular heterometallic framework of **I** along the *y* axis showing existence of 1D channels along the crystallographic *y* axis in porous title complex, guest water molecules are not presented for clarity (b).

sult is close to the theoretical value 4.49% for per $[Er_2Co_2(\mu_3\text{-HMimda})_2(\mu_3\text{-Mimda})_2 \cdot 4H_2O]_n \cdot 2nH_2O$. The second weight loss of 4.48% in the range of 220–240°C is attentively assigened to release of coordination waters. After the loss of water molecules, the 3D framework begins to decompose upon further heating. It also exhibits two exdothermic peaks with a total weight loss of 27.1%, the larger exothermic peak located at about 440°C, which was probably caused by the decomposition of [Er(HMimda)] moiety. The complex sketch begins obvious collapse beyond the temperature of 500°C.

The direct current (dc) magnetic susceptibilities for complex were measured using the polycrystalline samples of **I** in an applied dc field of 0.20 T. As depicted in Fig. 5, the $\chi_M T$ value is equal to 13.60

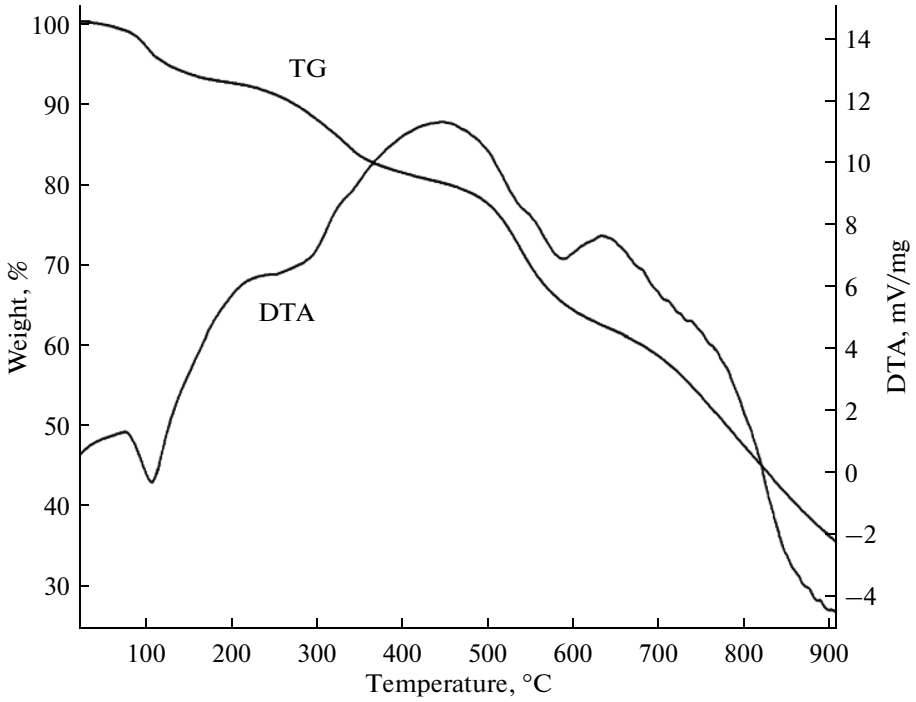

Fig. 4. TG–DTA curves for complex **I**.

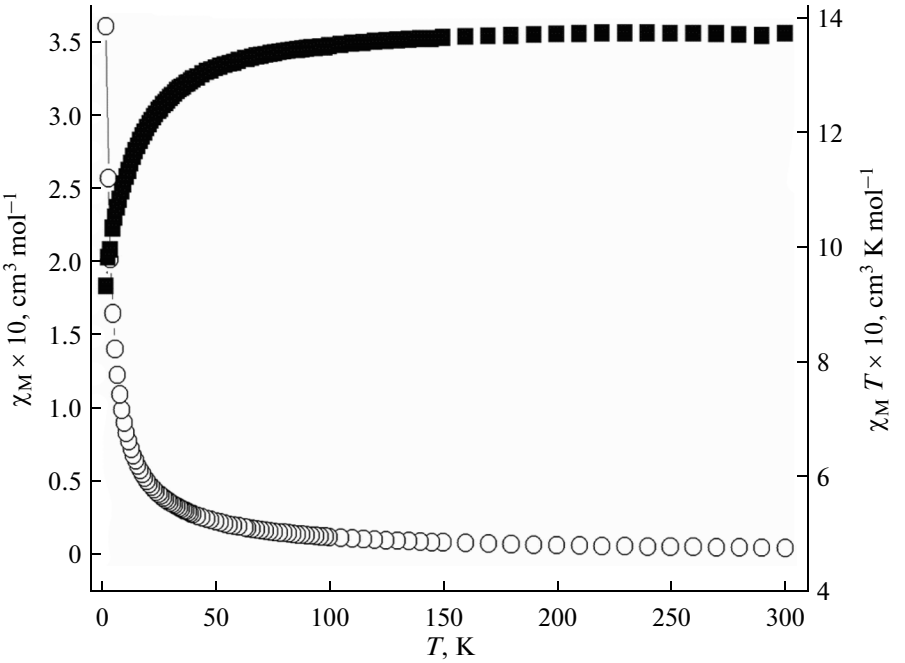

Fig. 5. Temperature dependence of the χ_M (■) and $\chi_M T$ (○) products at 0.20 T for complex **I**.

cm^3 K mol^{-1} for **I** at room temperature, which is close to the value expected for an isolated Er^{3+} ion (11.48 cm^3 K mol^{-1}) added to 1.87 cm^3 K mol^{-1} for a Co^{2+} ion [16]. As the temperature is lowered, $\chi_M T$ product decreases very gradually to a value of 9.32 cm^3 K mol^{-1} before at 60 K. For title complex, the $\chi_M T$ values display a sharp more pronounced decrease occurs below 50 K, reaching minimum value of 8.94 cm^3 K mol^{-1} at 2 K. The decrease $\chi_M T$ value in this case is attributed to the depopulation of the m_J sublevels of the ground J

multiplet with the possibility of weak antiferromagnetic exchange between Er^{3+} ions [17] and dipolar interactions also contributing to the behavior. This is mainly because of the splitting of the 10-fold degenerate $^4I_{9/2}$ ground state by the crystal field and the progressive depopulation of the higher energy, as the temperature is lowered. The presence of thermally populated excited state makes the magnetic property of the erbium title complex remains difficult to interpret, especially for high dimensional system.

ACKNOWLEDGMENTS

This work was supported by the National Natural Science Foundation of China (no. 21273101), the Foundation of the Program for Backbone Teachers in Universities of Henan Province (no. 2012GGJS158), tackle key problem of science and technology Project of Henan Province (no. 142102310483), and the Foundation of Education Committee of Henan Province (no. 14B150033), and Program for University of Malaya (UM.C/625/1/HIR/247).

REFERENCES

1. Zhao, B., Cheng, P., Chen, X.Y., et al., *J. Am. Chem. Soc.*, 2004, vol. 126, no. 10, p. 3012.
2. Xu, H.B., Zhong, Y.T., Zhang, W.X., et al., *Dalton Trans.*, 2010, vol. 39, p. 5676.
3. Luo, J.H., Xu, H.W., Liu, Y., et al., *J. Am. Chem. Soc.*, 2008, vol. 130, no. 30, p. 9626.
4. Feng, X., Ling, X.L., Liu, L., et al., *Dalton Trans.*, 2013, vol.42, p. 10292.
5. Zou, L.F., Zhao, L., Guo, Y.N., et al., *Chem. Commun.*, 2011, vol. 47, p. 8659.
6. Pasatoiu, T.D., Sutter, J.P., Madalan, A.M., and Andruh, M., *Inorg. Chem.*, 2011, vol. 50, no. 13, p. 5890.
7. Liu, Q., Ge, S.Z., Zhong, J.C., et al., *Dalton Trans.*, 2013, vol. 42, p. 6314.
8. Feng, X., Wang, J.G., Liu, B., et al., *Cryst. Growth Des.*, 2012, vol. 12, no. 2. p. 927.
9. Sheldrick, G.M., *SHELXS-97, Program for the Solution of Crystal Structure*, Göttingen (Germany): Univ. of Göttingen, 1997.
10. Sheldrick, G.M., *SHELXL-97, Program for the Crystal Structure Refinement*, Göttingen (Germany): Univ. of Göttingen, 1997.
11. Yang, X.Y., Yang, L.., Lei, P. P., et al., *Z. Kristallogr. NCS*, 2012, vol. 227, no. 1, p. 59.
12. Feltham, H.L.C., Lan, Y.H., Klöwer, A.F., et al., *Chem. Eur. J.*, 2011, vol. 17, no. 16, p. 4362.
13. Biju, S., Eom, Y.K., Bünzli, J.-C.G., et al., *J. Mater. Chem. C*, 2013, no. 21, p. 3454.
14. Feng, X., Ma, L.F., Liu, L., et al., *Cryst Growth Des.*, 2013, vol. 13, no. 10, p. 4469.
15. Spek, A.L., *J. Appl. Crystallogr.*, 2003, vol. 36, p. 7.
16. Shimada, T., Okazawa, A., Kojima, N., et al., *Inorg. Chem.*, 2011, vol. 50, no. 21, p. 10555.
17. Esplin, T.L., Cable, M.L., Gray, H.B., and Ponce, A., *Inorg. Chem.*, 2010, vol. 49, no. 9, p. 4643.